European Biophysics Journal (2019) 48:329–340
https://doi.org/10.1007/s00249-019-01357-4

ORIGINAL ARTICLE

Mechanical property of the helical configuration for a twisted intrinsically straight biopolymer

Zicong Zhou[1] · Chen-Xu Wu[2]

Received: 18 December 2018 / Revised: 1 March 2019 / Accepted: 8 March 2019 / Published online: 27 March 2019

Abstract

We explore the effects of two typical torques on the mechanical property of the helical configuration for an intrinsically straight filament or biopolymer either in three-dimensional space or on a cylinder. One torque is parallel to the direction of a uniaxial applied force, and is coupled to the cross section of the filament. We obtain some algebraic equations for the helical configuration and find that the boundary conditions are crucial. In three-dimensional space, we show that the extension is always a monotonic function of the applied force. On the other hand, for a filament confined on a cylinder, the twisting rigidity and torque coupled to the cross section are irrelevant in forming a helix if the filament is isotropic and under free boundary condition. However, the twisting rigidity and the torque coupled to the cross section become crucial when the Euler angle at two ends of the filament are fixed. Particularly, the extension of a helix can subject to a first-order transition so that in such a condition a biopolymer can act as a switch or sensor in some biological processes. We also present several phase diagrams to provide the conditions to form a helix.

Keywords Mechanical property · Twisted biopolymer · Helix · Phase transition

Introduction

A biopolymer is often modeled as an elastic filament owing to its chain structure. Conformational and mechanical properties of a filament have attracted a lot of attention for a long time owing to its wide range of applications in either macroscopic objects such as pillars or microscopic objects such as semiflexible biopolymers (Benham 1977, 1989; Tanaka and Takahashi 1985; Fain et al. 1997; Fain and Rudnick 1999; Panyukov and Rabin 2001; Zhou et al. 2005, 2007; Zhou 2018; Love 1944; Marko and Siggia 1994; Bustamante et al. 1994; Marko and Siggia 1998; Kratky and Porod 1949; Panyukov and Rabin 2000; Goriely and Shipman 2000; Kessler and Rabin 2003; Erickson et al. 1996; Srinivasan et al. 2008; Smith et al. 2001; Jones et al. 2001; Iwai et al. 2002; Daniel and Errington 2003; Gitai et al. 2004, 2005; Kruse et al. 2005; Carballido-López 2006; Vats and Rothfield 2007; van der Heijden 2001; Chouaieb et al. 2006; Allard and Rutenberg 2009; Zhou et al. 2017; Jung and Ha 2019; Panyukov and Rabin 2002; Shih et al. 2003; Taghbalout and Rothfield 2007; Thanedar and Margolin 2004; Vaillant et al. 2005; Esue et al. 2006; Andrews and Arkin 2007; Russell and Keiler 2007; Srinivasan et al. 2007; Zhou 2007; Moukhtar et al. 2007; Starostin and van der Heijden 2010; Zhou et al. 2014).

The configuration of a filament can be described by the shape of its centerline and the twist of its cross section around the centerline. Denoting the arc length of the centerline as s and the locus of centerline as $\mathbf{r}(s)$, the configuration of a filament can be described by a triad of unit vectors $\{\mathbf{t}_i\}_{i=1,2,3}$, in which $\mathbf{t}_3 \equiv \dot{\mathbf{r}}$ is the tangent to the center line, $\mathbf{t}_1$ and $\mathbf{t}_2$ are oriented along the principal axes of the cross section (Benham 1977, 1989; Tanaka and Takahashi 1985; Fain et al. 1997; Fain and Rudnick 1999; Panyukov and Rabin 2001; Zhou et al. 2005, 2007; Zhou 2018) and the symbol "." represents the derivative with respect to s. $\{\mathbf{t}_i\}_{i=1,2,3}$ satisfy the generalized Frenet equations $\dot{\mathbf{t}}_i = \boldsymbol{\omega} \times \mathbf{t}_i$ (Benham 1977, 1989; Tanaka and Takahashi 1985; Fain et al. 1997; Fain and Rudnick 1999; Panyukov and Rabin 2001; Zhou et al.

✉ Zicong Zhou
zzhou@mail.tku.edu.tw

Chen-Xu Wu
cxwu@xmu.edu.cn

1 Department of Physics, Tamkang University, 151 Yingzhuan Road, Tamsui Dist., New Taipei City 25137, Taiwan, China

2 Department of Physics and ITPA, Xiamen University, Xiamen 361005, Fujian, China

2005, 2007; Zhou 2018), and the vector $\boldsymbol{\omega} = (\omega_1, \omega_2, \omega_3)$ represents curvature and torsion parameters (Benham 1977, 1989 Tanaka and Takahashi 1985; Fain et al. 1997; Fain and Rudnick 1999; Panyukov and Rabin 2001; Zhou et al. 2005, 2007; Zhou 2018).

Moreover, intrinsic properties and external conditions determine the conformal and mechanical properties of a filament. The intrinsic properties are usually referred to as bending rigidities, twisting rigidity and inertia tensor (Benham 1977; Tanaka and Takahashi 1985; Fain et al. 1997; Fain and Rudnick 1999; Panyukov and Rabin 2001; Zhou et al. 2005, 2007; Zhou 2018; Love 1944). On the other hand, external physical conditions include applied forces, torques and constraints such as boundary conditions (BCs) or confinements. To explore different physical properties, it usually requires different models. For instance, regarding a filament as an inextensible chain with a finite bending rigidity but a zero cross-section area leads to the wormlike chain (WLC) model, and it has been applied to describe the entropic elasticity of some semiflexible biopolymers (Marko and Siggia 1994; Bustamante et al. 1994; Marko and Siggia 1998; Kratky and Porod 1949). Another simple model is the wormlike rod chain (WLRC) model which views a filament as a chain of a finite intrinsic twist and an isotropic cross section (Fain et al. 1997; Marko and Siggia 1994; Bustamante et al. 1994; Marko and Siggia 1998). Both WLC and WLRC models are intrinsically straight, i.e., free of external force and torque, and their ground-state configurations (GSCs, or the configuration with the lowest energy) are either a straight line or a straight cylinder, respectively. In contrast, the unique GSC of an intrinsically curved filament gives a curved centerline with a given curvature when it is free of external force and torque.

A filament can form various structures and the simplest but very useful one is a helix. A helix may result from a finite intrinsic curvature and torsion (Zhou et al. 2005, 2007; Zhou 2018; Panyukov and Rabin 2000; Goriely and Shipman 2000; Kessler and Rabin 2003; Erickson et al. 1996; Srinivasan et al. 2008; Smith et al. 2001). Free of external force or torque, such a filament has naturally a helical shape and can maintain the helix under a uniaxial force (Zhou et al. 2005, 2007; Panyukov and Rabin 2000; Goriely and Shipman 2000; Kessler and Rabin 2003). In contrast, under a uniaxial force to have a helical shape, an intrinsically straight filament requires some external torques or constraints, such as a MreB molecule inside a cylindrical bacteria (Jones et al. 2001; Iwai et al. 2002; Daniel and Errington 2003; Gitai et al. 2004, 2005; Kruse et al. 2005; Carballido-López 2006; Vats and Rothfield 2007). The elasticity of a helix, either in three-dimensional (3D) space or on the surface of a cylinder, has been studied extensively (Zhou et al. 2005, 2007; Zhou 2018; Love 1944; Panyukov and Rabin 2000; Goriely and Shipman 2000; Kessler and Rabin 2003; van der Heijden 2001; Chouaieb et al. 2006; Allard and Rutenberg 2009; Zhou et al. 2017; Jung and Ha 2019). However, a full picture on the conditions to form a helix for an intrinsically straight filament is yet elusive. Particularly, the roles of different torques are not yet transparent. Moreover, it has been reported that under an applied force, the extension of a filament can subject to a sharp transition for either an intrinsically curved filament in 3D space or an intrinsically straight filament confined on a cylinder (Zhou et al. 2005, 2007; Zhou 2018; Allard and Rutenberg 2009; Zhou et al. 2017). Two relevant questions are then intrigue. The first one is that would torques also induce the same behavior, and the second is what kind of torque would have stronger effect for the transition? In this work, we find some algebraic static equations for a helix to obtain some exact results to answer these questions. We study the effects of two typical torques, one is parallel to the direction of a uniaxial applied force and another is coupled to the cross section of the filament. We show that BCs affect the results seriously. In 3D space, we find that the extension increases monotonically with increasing force so that there is not abrupt transition. However, for a confined filament with a fixed BC, the extension can subject to a first-order phase transition. We also present several phase diagrams to provide conditions to form a helix. Our findings suggest that under some conditions, an intrinsically straight semiflexible biopolymer can also act as a switch or sensor in some biological processes. Moreover, note that the fixed BC is analogous to prestressing a filament and in engineering, such as to build houses or bridges, it is commonly to use prestressed steel wires, the effect of a fixed BC may be instructive to engineering.

The paper is organized as follows. In the next section, we set up elastic models for an intrinsically straight filament. It follows a section on the mechanical property of a helix in 3D space. In Sect. 4, we focus on a helix confined on a cylinder. The section with conclusions and discussions completes the main text of the paper. Finally, we provide a appendix to discuss how to realize torques used in this work.

Models

Energy of a filament in 3D space

The configuration of a filament is analogous to the trajectory of a rigid plate so that we can use Euler angles θ, ϕ and ψ, as shown in Fig. 1, to describe it (Tanaka and Takahashi 1985; Benham 1989; Fain et al. 1997; Fain and Rudnick 1999; Panyukov and Rabin 2001; Zhou et al. 2005, 2007; Zhou 2018). It follows (Goldstein 2002)

$$\mathbf{t}_3 = (\sin\phi\sin\theta, -\cos\phi\sin\theta, \cos\theta), \tag{1}$$

$$\omega_1 = \sin\theta\sin\psi\ \dot{\phi} + \cos\psi\ \dot{\theta}, \tag{2}$$

$$\omega_2 = \sin\theta\cos\psi\ \dot{\phi} - \sin\psi\ \dot{\theta}, \tag{3}$$

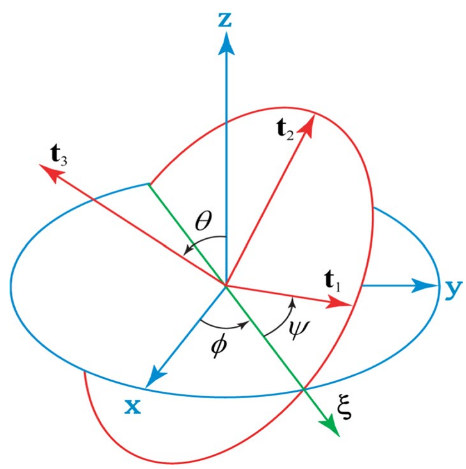

Fig. 1 Definition of the Eulerian angles. ξ is the line of nodes which is a line perpendicular to tangent of the centerline and lies on the horizontal plane of the fixed frame. x, y and z are unit vectors on the axis of the fixed coordinate system

$$\omega_3 = \cos\theta\,\dot{\phi} + \dot{\psi}. \tag{4}$$

and $\mathbf{r}(s) = (x, y, z) = \int_0^s \mathbf{t}_3(u)\mathrm{d}u$. The main advantage of using Euler angles is that we can find some algebraic static equations and so can obtain some exact results.

In this work, we focus on two kinds of torque which are relatively easier to realize. Both torques are applied to $s = L$. The first one is N_z which is along the direction of z-axis, and gives an energy density $N_z(\dot{\phi} + \cos\theta\dot{\psi})$, as derived in Appendix. The second one is N_3 which is along the axis of filament, and provides an energy density $N_3\omega_3$, as derived in Appendix. For simplicity, we study their effects separately in this work, but it is easy to find more complicate results since we provide algebraic static equations.

In 3D space, the energy of an intrinsically straight and uniform filament with an intrinsic twist rate ω_0 can be written as

$$E = \int_0^L \mathcal{E}\mathrm{d}s, \tag{5}$$

$$\mathcal{E} = \mathcal{E}_0 - F\cos\theta - N_z(\dot{\phi} + \cos\theta\dot{\psi}) - N_3\omega_3, \tag{6}$$

$$\mathcal{E}_0 = \frac{k_1}{2}\omega_1^2 + \frac{k_2}{2}\omega_2^2 + \frac{k_3}{2}\left(\omega_3 - \omega_0\right)^2, \tag{7}$$

where k_1 and k_2 are bending rigidities, k_3 is twisting rigidity, F is an uniaxial force along z-axis, L is the total contour length and is a constant; i.e., we consider an inextensible filament. F is also applied to $s = L$. When $k_1 = k_2$, the filament is isotropic or has a circular cross section. When $k_1 = k_2$ and $N_z = 0$, it recovers the usual form of WLRC model (Fain et al. 1997; Marko and Siggia 1994; Bustamante et al. 1994; Marko and Siggia 1998).

Replacing N_3 by $N_3' = N_3 + k_3\omega_0$, $\mathcal{E}$ becomes

$$\begin{aligned}\mathcal{E} = {} & \frac{k_1}{2}\omega_1^2 + \frac{k_2}{2}\omega_2^2 + \frac{k_3}{2}\omega_3^2 - F\cos\theta \\ & - N_z(\dot{\phi} + \cos\theta\dot{\psi}) - N_3'\omega_3 + \frac{k_3}{2}\omega_0^2.\end{aligned} \tag{8}$$

Therefore, in fact ω_0 can be merged with N_3, so that we will ignore ω_0 henceforth. Moreover, in numerical calculations and figures, we take $k_1 = 1$ for simplicity.

Energy of a filament confined on a cylinder

Let the axis of the cylinder be along the z-axis, confining a filament on the surface of a cylinder of radius R applies a constraint on the coordinates so that $x = R(1 - \cos\phi)$ and $y = -R\sin\phi$, as derived in Appendix. Comparing with Eq. (1), we obtain $\dot{\phi} = \sin\theta/R$ (Allard and Rutenberg 2009; Zhou et al. 2017). Applying a force, which is perpendicular to z-axis, at $\mathbf{r}(L)$ results in a torque along the z-axis, and an energy density $N_z\dot{\phi}$, as derived in Appendix. The energy for the filament confined on a cylinder is therefore

$$E = \int_0^L \mathcal{E}\mathrm{d}s, \tag{9}$$

$$\mathcal{E} = \mathcal{E}_0 - F\cos\theta - N_z\sin\theta/R - N_3\omega_3, \tag{10}$$

where N_3 is the same as that in Eq. (6), but N_z has a different meaning from that in Eq. (6). This is because N_z in Eq. (10) comes from a single force but to form the N_z in Eq. (6) requires a pair of forces, as we can see from Appendix. When $N_3 = 0$, the model with free BC has been studied extensively (Allard and Rutenberg 2009; Zhou et al. 2017), but the role of N_3 is yet unclear.

For simplicity, henceforth for a filament confined on a cylinder we will scale all lengths by R and the force by k_1/R^2, which corresponds to letting $R = 1$ and $k_1 = 1$ in E. The units of energy and torque are therefore k_1/R.

Definition of a helix

In terms of Eulerian angles, the curvature κ and torsion τ of a filament are (Zhou 2018)

$$\kappa = \sqrt{\dot{\theta}^2 + \sin^2\theta\dot{\phi}^2}, \tag{11}$$

$$\tau = \cos\theta\dot{\phi} + \frac{\sin\theta(\dot{\theta}\ddot{\phi} - \dot{\phi}\ddot{\theta}) + \cos\theta\dot{\phi}\dot{\theta}^2}{\kappa^2}. \tag{12}$$

Note that in general $\tau \neq \omega_3$ (Zhou 2018).

A general helix is defined as a curve in which $\mathbf{t}_3$ makes a constant angle with a fixed direction. This condition is equivalent to having a s-independent κ/τ. In this work, we always apply a force along z-axis, so that the symmetry implies that θ is s-independent. Therefore, we define the relative extension as $z_r \equiv z(L)/L = \cos\theta$ for a helix. Without loss of generality, we also choose $1 \geq z_r \geq 0$. When both κ and τ are s-independent, the helix is called a circular helix.

Static equations

In this work, we focus on GSCs. For a short rigid filament, the thermal effect is less important unless in some critical cases, since the rigidity tends to depress configurational fluctuation, so that at a first approximation we can ignore thermal fluctuation and find the GSCs by minimizing energy. Applying the standard variational technique results in the following static equations:

$$\frac{\partial \mathcal{E}}{\partial \theta} - \frac{d}{ds}\frac{\partial \mathcal{E}}{\partial \dot{\theta}} = \frac{\partial \mathcal{E}}{\partial \phi} - \frac{d}{ds}\frac{\partial \mathcal{E}}{\partial \dot{\phi}} = \frac{\partial \mathcal{E}}{\partial \psi} - \frac{d}{ds}\frac{\partial \mathcal{E}}{\partial \dot{\psi}} = 0, \tag{13}$$

and boundary conditions (BCs) at $s = 0$ and $s = L$

$$\frac{\partial \mathcal{E}}{\partial \dot{\theta}}\delta\theta = \frac{\partial \mathcal{E}}{\partial \dot{\phi}}\delta\phi = \frac{\partial \mathcal{E}}{\partial \dot{\psi}}\delta\psi = 0. \tag{14}$$

On a cylinder, we ignore the equations related to ϕ and $\dot{\phi}$ in Eqs. (13)–(14).

Physically, for an arbitrary variable X, $\delta X(x) = 0$ means to fix X at x. Therefore, $\delta\phi(L) = 0$ corresponds to fix $\phi(L)$ but $\partial\mathcal{E}/\partial\dot{\phi}|_{s=L} = 0$ corresponds to have a free $\phi(L)$. In variational method, to fix $X(0)$ and $X(L)$ is equivalent to introduce an effective term $-\alpha_X \dot{X}$ in energy density where α_X, such as C_ϕ or C_ψ used hereafter, is a BC-dependent constant and is the generalized force required to fix X. In other words, to realize these constraints requires some complicate forces. Note that under a finite torque, to have a static configuration it is always necessary to fix $\phi(0)$ and $\psi(0)$ so that we always take $\delta\phi(0) = \delta\psi(0) = 0$. We also do not fix $\theta(0)$ and $\theta(L)$ in this work, since owing to the choice of F, a helix requires a s-independent θ so it satisfies $\partial\mathcal{E}/\partial\dot{\theta} = \dot{\theta} = 0$ at both $s = 0$ and $s = L$ automatically.

For a biopolymer, fixing $\phi(L)$ or $\psi(L)$ can be realized by binding two ends with some molecules. From Fig. 1, we know that to fix $\phi(L)$ means to fix the line of nodes at $s = L$, and the cross section of the filament can still rotate around $\mathbf{t}_3$. On the other hand, fixing $\psi(L)$ requires to specify a line on the cross section as the line of nodes, but the line of nodes can still rotate around z-axis.

When torques and BCs are given, a stable configuration requires $g \equiv \mathrm{d}F/\mathrm{d}z_r > 0$ or extension increases with increasing force. Moreover, if g has more than one real zeros, there will be an abrupt change in z_r (Zhou et al. 2005, 2007; Zhou 2018; Zhou et al. 2017).

Mechanical property of a helix in 3D space

When $k_1 = k_2$

In this case, Eq. (13) becomes

$$[(k_3 - k_1)\cos\theta\dot{\phi}^2 - (N_3 - k_3\dot{\psi})\dot{\phi} - N_z\dot{\psi} - F]\sin\theta + k_1\ddot{\theta} = 0, \tag{15}$$

$$k_3 z_r \dot{\psi} + (k_3\cos^2\theta + k_1\sin^2\theta)\dot{\phi} - N_z - N_3\cos\theta = C_\phi, \tag{16}$$

$$k_3(\dot{\psi} + \cos\theta\dot{\phi}) - N_z\cos\theta - N_3 = C_\psi, \tag{17}$$

and BC for θ is $\dot{\theta} = 0$ at both $s = 0$ and $s = L$.

From Eqs. (15)–(17), we know that $\ddot{\theta}$, $\dot{\theta}$, $\dot{\phi}$ and $\dot{\phi}$ can all be expressed as functions of θ. Therefore, from Eqs. (11)–(12), requiring κ/τ be s-independent results in a s-independent θ. It follows that $\dot{\phi}$ and $\dot{\psi}$ are also s-independent so we obtain some algebraic static equations.

With free BCs

In this case $C_\phi = C_\psi = 0$, so from Eqs. (15)–(17), it is straightforward to find that for a helix

$$F = N_z[-k_1 N_3 + (k_3 - k_1)N_z z_r]/k_1 k_3. \tag{18}$$

Therefore, to form a helix, a finite N_z is a necessity but N_3 can be zero and it is also irrelevant to stability. Moreover, F is a linear function of z_r, i.e., the filament becomes a Hooke's spring, and when $k_3 > k_1$, a helix is stable, but if $k_1 > k_3$, a helix is always unstable.

When $\phi(L)$ is fixed

Now we consider the case with a fixed $\phi(L)$ but a free $\psi(L)$ so $C_\psi = 0$. In this case, $\dot{\phi} = [\phi(L) - \phi(0)]/L$ is determined by BC, and from Eqs. (15)–(17), we find

$$F = -[N_z N_3 + (N_z^2 - 2k_3 N_z\dot{\phi} + k_1 k_3\dot{\phi}^2)z_r]/k_3, \tag{19}$$

$$g = -(N_z^2 - 2k_3 N_z\dot{\phi} + k_1 k_3\dot{\phi}^2)/k_3. \tag{20}$$

From Eqs. (19)–(20), we know that F is also a linear function of z_r and a large N_z or $\dot{\phi}$ makes a helix unstable. From Eq. (20), we can show exactly that when $k_1 > k_3$, a helix is always unstable since $g < 0$, and when $k_3 > k_1$, a helix is stable only when $N^+ > N_z > N^-$ with $N^\pm = [k_3 \pm \sqrt{k_3(k_3 - k_1)}]\dot{\phi}$. N_3

is still irrelevant to stability. Comparing with the results for free BCs, fixing $\phi(L)$ is not a proper way to form a helix since it can form a Hooke's spring in a limited range of N_z only so it is uneasy to realize.

When $\boldsymbol{\Omega}(L)$ is fixed

Next, we consider the case with a fixed $\psi(L)$ but a free $\phi(L)$ so $C_\phi = 0$. In this case, $\dot\psi = [\psi(L) - \psi(0)]/L$ is s-independent and from Eqs. (15)–(17), we obtain

$$\dot\phi = [N_z + (N_3 - k_3\dot\psi)z_r]/[k_1 + (k_3 - k_1)z_r^2]. \tag{21}$$

$$\begin{aligned} F = \big[&-k_1N_z[N_3 - (k_3 - k_1)\dot\psi] \\ &+ [(k_3 - k_1)N_z^2 - k_1(N_3 - k_3\dot\psi)^2]z_r \\ &+ (k_3 - k_1)N_z[N_3 - (2k_1 + k_3)\dot\psi]z_r^2 \\ &-(k_3 - k_1)^2N_z\dot\psi z_r^4\big]/\big[k_1 + (k_3 - k_1)z_r^2\big]^2. \end{aligned} \tag{22}$$

From Eq. (22), we find that when $N_z = 0$,

$$g = -\frac{k_1[k_1 + 3(k_1 - k_3)z_r^2](N_3 - k_3\dot\psi)^2}{[k_3z_r^2 + k_1(1 - z_r^2)]^3}. \tag{23}$$

Therefore, when $k_3 < 4k_1/3$, a helix is unstable but when $k_3 > 4k_1/3$, a helix is stable if $z_r > z_1 \equiv \sqrt{k_1/(3k_3 - 3k_1)}$.

In contrast, when $N_3 = 0$, from Eq. (22) we obtain

$$\begin{aligned} g = N_z^2\{&k_1[(k_1 - k_3) + k_1k_3^2\gamma^2] - 6k_1k_3(k_1 - k_3)\gamma z_r \\ &+ 3(k_1 - k_3)[(k_1 - k_3) + k_1k_3^2\gamma^2]z_r^2 \\ &- 2(k_1 - k_3)^2k_3\gamma z_r^3\}[(k_1 - k_3)z_r^2 - k_1]^{-3}, \end{aligned} \tag{24}$$

where $\gamma = \dot\psi/N_z$.

From Eq. (24), we find that when $\dot\psi = 0$, $g = N_z^2(k_3 - k_1)[k_1 + 3(k_1 - k_3)z_r^2]/[k_1 + (k_3 - k_1)z_r^2]^3$ so that $g < 0$ when $k_3 < k_1$. In contrast, when $k_3 > k_1$, a helix is stable if $z_r < z_1$. It follows that when $k_3 > 4/3k_1$, a helix is unstable at large z_r since $z_1 < 1$, but if $k_3 < 4/3k_1$, a helix is stable since $z_1 > 1$.

When $N_3 = 0$ but $\gamma \neq 0$, $g = -k_1\dot\psi^2 \leq 0$ when $k_3 = k_1$ so that a helix is unstable. Furthermore, it is straightforward to show that $dg/dz_r = 0$, $d^2g/dz_r^2 < 0$ and $g < 0$ at $z_r = z_0 = k_3\gamma/(k_3 - k_1)$ when $k_3 < k_1$. In other words, $g < 0$ and g reaches maximum at z_0 when $k_3 < k_1$. Consequently, to form a helix, it requires $k_3 > k_1$.

Moreover, from Eq. (24), we find that when $N_3 = 0$, the phase diagram, Fig. 2, for a helix can be divided into six regimes separated by $\gamma_0^\pm$, $\gamma_1^\pm$, $k_3 = k_1$ and $k_3 = 4k_1$, with

$$\gamma_0^\pm = \pm\sqrt{k_3 - k_1}/(k_3\sqrt{k_1}), \tag{25}$$

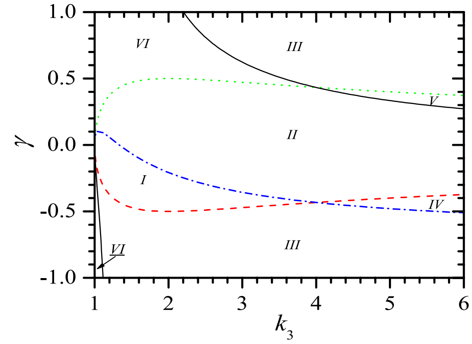

Fig. 2 Phase diagram for a helix when $k_1 = k_2 = 1$ and $N_3 = 0$. γ_0^- (red dashed), γ_0^+ (green dotted), γ_1^- (black solid) and γ_1^+ (blue dash dotted) are plotted

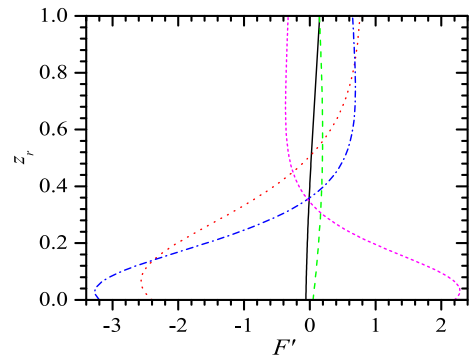

Fig. 3 z_r vs $F' \equiv F/N_z^2$ when $k_3 = 1.2$ and $\gamma = -0.3$ (black solid); $k_3 = 1.5$ and $\gamma = 0.1$ (green dashed); $k_3 = 5$ and $\gamma = -0.6$ (red dotted); $k_3 = 9$ and $\gamma = -0.4$ (blue dash dotted); $k_3 = 12$ and $\gamma = 0.2$ (magenta short dashed). $k_1 = k_2 = 1$ and $N_3 = 0$ in all cases

$$\gamma_1^\pm = \frac{(k_3 - k_1)(k_3 - 4k_1) \pm k_3^{3/2}\sqrt{k_3 - k_1}}{k_1k_3(4k_1 - 3k_3)}. \tag{26}$$

$g = 0$ at $z_r = 0$ or $z_r = 1$ when $\gamma = \gamma_0^\pm$ or $\gamma = \gamma_1^\pm$, respectively. Consequently, when γ is far from $\gamma = \gamma_0^\pm$, a helix with small z_r may be unstable; when γ is far from $\gamma = \gamma_1^\pm$, a helix with large z_r may be unstable.

In regime I, a helix is always stable since $g > 0$ and it occurs when $4k_1 > k_3 > k_1$ and $\gamma_1^+ > \gamma > \gamma_0^-$. In other words, to form a helix at any z_r, k_3 and $|\gamma|$ cannot be too large. A typical sample is shown as the black solid line in Fig. 3.

In regime II, $g > 0$ or a helix is stable when $z_{\mathrm{II}} > z_r > 0$ and it occurs when $4k_1 > k_3 > k_1$ and $\gamma_0^+ > \gamma > \gamma_1^+$ or $k_3 > 4k_1$ and $\gamma_1^- > \gamma > \gamma_0^-$. $z_{\mathrm{II}} < 1$ so that a helix of large z_r cannot exist. The value of z_{II} is dependent on k_3 and γ. The green dashed line in Fig. 3 shows a typical sample in regime *II*.

In regime III, a helix is stable when $1 > z_r > z_{\rm III} > 0$ and it occurs in three cases. The first case requires $4/3k_1 > k_3 > k_1$ and $\gamma_0^- > \gamma > \gamma_1^-$ simultaneously; the second case needs $4k_1 > k_3 > 4/3k_1$ and $\gamma_0^- > \gamma$ or $\gamma > \gamma_1^-$; and the third case requires $k_3 > 4k_1$ and $\gamma < \gamma_1^+$ or $\gamma > \gamma_0^+$. A helix of small z_r cannot exist in this regime. The red dotted line in Fig. 3 shows a typical sample in the regime. The value of $z_{\rm III}$ is also dependent on k_3 and γ.

In regime IV, a helix is stable when $z^1_{\rm IV} > z_r > z^0_{\rm IV}$ and it occurs when $k_3 > 4k_1$ and $\gamma_0^- > \gamma > \gamma_1^+$. The blue dash dotted line in Fig. 3 shows a typical sample in regime *IV*. The values of $z^0_{\rm IV}$ and $z^1_{\rm IV}$ are also dependent on k_3 and γ.

In regime V, a helix is stable when $z_r > z^1_{\rm V}$ or $z_r < z^0_{\rm V}$, with $z^1_{\rm V} > z^0_{\rm V}$ and it occurs when $k_3 > 4k_1$ and $\gamma_0^+ > \gamma > \gamma_1^-$. The magenta short dashed line in Fig. 3 shows a typical sample in regime *V*. But note that in this regime, the force in $z_r < z^0_{\rm V}$ is larger than that in $z_r > z^1_{\rm V}$, which means that a larger force would result in a smaller z_r, so that these two branches cannot be both in stable states, but one of which should be in a metastable state.

Finally, in regime *VI*, there is not helix and it occurs when $4/3k_1 > k_3 > k_1$ and $\gamma_1^- > \gamma$ or $\gamma > \gamma_0^+$, or $4k_1 > k_3 > k_1$ and $\gamma_1^- > \gamma > \gamma_0^+$. In other words, a negative or large γ but a small k_3 does not favor a helix.

In summary, when $k_1 = k_2$, to have a stable helix requires $k_3 > k_1$. The relation between F and z_r is dependent on BCs. With free BC or fixing $\phi(L)$, the helix is a Hooke's spring and N_3 is irrelevant. In other words, when $\psi(L)$ is free, the twist around the cross section is decoupled from the bending of the centerline. Fixing $\phi(L)$ also makes a helix stable only in a limited range of N_z so it is not a proper way to realize a helix. On the other hand, fixing $\psi(L)$ results in a non-Hooke's helix which may exist only in a certain range of z_r and it requires a complicate relation between γ and k_3. In all cases, F is a monotonic function of z_r so that there is not any abrupt change in z_r.

When $k_1 \neq k_2$

When $k_1 \neq k_2$, there is not a direct way to show exactly that θ must be s-independent for a helix. However, note that both F and N_z are along z-axis and the main role of N_3 is to distort the cross section so should affect less on shape of the centerline; from symmetry, it is reasonable to expect that the axis of a helix is also along z-axis so that θ is also s-independent. Consequently, Eq. (13) is reduced into

$$\begin{aligned}&(k_1-k_2)\sin(2\psi)\ddot{\phi} - 2N_z\dot{\psi} - 2F\\&\quad - 2[N_3 - (k_3 + (k_1-k_2)\cos(2\psi))\dot{\psi}]\dot{\phi}\\&\quad + z_r[2k_3 - k_1 - k_2 + (k_1-k_2)\cos(2\psi)]\dot{\phi}^2 = 0,\end{aligned} \tag{27}$$

$$\begin{aligned}&[k_3 z_r^2 + k_2(1-z_r^2)\cos^2\psi + k_1(1-zr^2)\sin^2\psi]\dot{\phi}\\&\quad + k_3 z_r\dot{\psi} - N_z - N_3 z_r = C_\phi,\end{aligned} \tag{28}$$

$$2k_3(z_r\ddot{\phi} + \ddot{\psi}) - (k_1-k_2)(1-z_r^2)\sin(2\psi)\dot{\phi}^2 = 0. \tag{29}$$

with BCs

$$\sin(2\psi)\dot{\phi}\delta\theta = 0, \tag{30}$$

$$\left[k_3(\dot{\psi} + z_r\dot{\phi}) - N_3 - N_z z_r\right]\delta\psi = 0. \tag{31}$$

Equations (27)–(29) are second-order nonlinear differential equations of ϕ and ψ. It is straightforward to show that in general these equations are incompatible if $\ddot{\phi} \neq 0$ or $\ddot{\psi} \neq 0$. Therefore, to form a helix, it requires $\ddot{\phi} = \ddot{\psi} = 0$ and it follows $\psi = 0$ or $\psi = \pi/2$ from Eq. (29). Moreover, we can show that taking $\psi = \pi/2$ is equivalent to taking $\psi = 0$ and exchanging k_1 and k_2 in Eqs. (27)–(28). In other words, for a helix we only need to consider the case with $\psi = 0$.

It is also straightforward to show that when both $\phi(L)$ and $\psi(L)$ are free, Eq. (31) is inconsistent with Eq. (28) so that there is not stable helix.

With free $\phi(L)$

With free $\phi(L)$ so $C_\phi = 0$, taking $\psi = \psi(L) = 0$, from Eqs. (27)–(31) we obtain

$$\dot{\phi} = (N_z + N_3 z_r)/[k_2 + (k_3-k_2)z_r^2], \tag{32}$$

$$F = \frac{(N_z + N_3 z_r)[(k_3-k_2)N_z z_r - k_2 N_3]}{[k_2 + (k_3-k_2)z_r^2]^2}. \tag{33}$$

When $N_z = 0$,

$$g = \frac{k_2 N_3^2[-k_2 + 3(k_3-k_2)z_r^2]}{[k_3 z_r^2 + k_2(1-zr^2)]^3}. \tag{34}$$

Meanwhile, when $N_3 = 0$,

$$g = \frac{N_z^2(k_3-k_2)(k_2 + 3(k_2-k_3)z_r^2)}{[k_3 z_r^2 + k_2(1-zr^2)]^3}. \tag{35}$$

It follows that when $k_3 < k_2$, $g < 0$ so that a helix is unstable in either $N_3 = 0$ or $N_z = 0$. A helix can be stable only when $1 \geq z_r > \sqrt{k_2/3(k_3-k_2)}$ and $k_3 > 4k_2/3$ if $N_z = 0$, or when $z_r < \sqrt{k_2/3(k_3-k_2)}$ if $N_3 = 0$. Therefore, N_z plays an opposite role to N_3 in this case. Moreover, g has only one zero for $1 > z_r > 0$ so that F is a smooth function of z_r.

When $\phi(L)$ is fixed

On the other hand, when $C_\phi \neq 0$ but $\psi = 0$, $\dot{\phi}$ is s-independent and Eqs. (27)–(31) result in

$$\dot{\phi} = (N_3 + N_z z_r)/k_3 z_r, \tag{36}$$

$$F = (N_3 + N_z z_r)[(k_3 - k_2)N_z z_r - k_2 N_3]/k_3^2 z_r. \tag{37}$$

When $N_z = 0$, $F = -k_2 N_3^3/k_3^2 z_r < 0$ is a compressive force and a helix is stable at arbitrary k_2 and k_3.

When $N_3 = 0$, $F = (k_3 - k_2)N_z^2 z_r/k_3^2$ so that to form a helix requires $k_3 > k_2$.

In summary, with free BCs, anisotropy prohibits a helix. With fixing $\phi(L)$, the filament becomes a non-Hooke's spring which may exist only in a certain range of z_r. In all cases, F is a monotonic function of z_r so that there is not abrupt change in z_r.

Mechanical properties of a helix confined on a cylinder

On a cylinder or inside a cell, binding two ends of a biopolymer is more feasible than that in 3D space, so that how to form a helix on a cylinder should be a more intrigue issue.

When $k_1 = k_2$

From Eq. (13), we obtain the following static equations

$$\dot{\psi} = N_3/k_3 - \sin\theta\cos\theta + C_\psi, \tag{38}$$

$$\begin{aligned} 4k_1\ddot{\theta} = {} & 4k_3\cos(2\theta)\dot{\psi} + (k_3 - k_1)\sin(4\theta) + 2k_1\sin(2\theta) \\ & + 4F\sin\theta - 4N_z\cos\theta - 4N_3\cos(2\theta). \end{aligned} \tag{39}$$

Similar to the 3D case, from Eqs. (38)–(39), we find that $\ddot{\theta}$, $\dot{\theta}$, $\ddot{\psi}$ and $\dot{\psi}$ can be expressed as functions of θ, so that requiring κ/τ be s-independent results in a s-independent θ. It follows that $\dot{\psi}$ is also s-independent so we obtain two algebraic equations again.

When $\psi(L)$ is free, $C_\psi = 0$ and

$$k_1\ddot{\theta} = 2k_1\sin^3\theta\cos\theta + F\sin\theta - N_z\cos\theta. \tag{40}$$

Equation (40) indicates that θ is independent of k_3 and N_3, or k_3 and N_3 do not affect the shape of the centerline so they can be ignored. N_3 affects only the twist around the centerline. It suggests that to obtain a helix, applying a N_z is an easier and more efficient way. The relevant system with a moderate length has been studied extensively (Allard and Rutenberg 2009; Zhou et al. 2017), and the main conclusions are (Zhou et al. 2017): Thermal effect and excluded volume interaction are less important; a uniaxial force results in a helix of large z_r only, and at a critical F the filament can collapse from a helix to a non-helix; N_z alone is enough to stabilize a helix to a very small z_r, and confinements from both ends reduce N_z effectively. Finally, there is not abrupt transition in extension between helices of different z_r.

Owing to thermal fluctuation, at a finite temperature BCs affect little a long filament. Consequently, at a finite temperature, k_3 and N_3 can be ignored for a long filament confined on a cylinder.

However, a semiflexible biopolymer may be short so that it is unreasonable to ignore BCs or k_3 and N_3. For instance, a MreB helix inside a cylindrical bacteria has only few turns (Jones et al. 2001; Iwai et al. 2002; Daniel and Errington 2003; Gitai et al. 2004, 2005; Kruse et al. 2005; Carballido-López 2006; Vats and Rothfield 2007). Therefore, we still need to consider the case with a fixed $\psi(L)$ and find it yields quite different results. In this case, we have

$$\begin{aligned} F = {} & [N_z z_r - N_3'(1 - 2z_r^2)]/\sqrt{1 - z_r^2} \\ & + [k_3 - 2k_1 + 2(k_1 - k_3)z_r^2]z_r. \end{aligned} \tag{41}$$

$$2\mathcal{E} = 1 + (N_3'^2 - N_3^2)/k_3 + 2z_r^2 - 3z_r^4 - \frac{2(N_z + N_3' z_r^3)}{\sqrt{1 - z_r^2}}. \tag{42}$$

$N_3' \equiv N_3 - k_3\dot{\psi}$ is an effective torque or fixing $\dot{\psi}$ plays a similar role as applying a finite N_3. But note that N_3 gives an additional constant in $\mathcal{E}$.

Equation (41) suggests that k_3 and N_3' are important for a helix, and a positive N_z or N_3' favors a helix. Moreover, when $z_r = 0$, $g = k_3 + N_z - 2k_1$ so that when $N_z + k_3 < 2k_1$, a helix with a small z_r is unstable. When $z_r \to 1$, $g \to (N_3' + N_z)/\sqrt{1 - z_r^2}$ so that a helix with a large z_r is stable if $N_3' + N_z > 0$.

When $N_z = 0$,

$$g = k_3 - 2k_1 + 6(k_1 - k_3)z_r^2 + \frac{N_3'(3 - 2z_r^2)z_r}{(1 - z_r^2)^{3/2}}. \tag{43}$$

Equation (43) results in $g < 0$ when $k_1 > k_3 > 0.8k_1$ and $N_3' < 0$. When $z_r = 0$, $g = k_3 - 2k_1$ so that it requires $k_3 > 2k_1$ to form a helix at small z_r. In another limit, $z_r \sim 1$, the sign of g is determined by N_3' and it requires $N_3' > 0$ to have a helix at large z_r. When $N_3' = 0$, $g > 0$ if $z_r < \sqrt{(k_3 - 2k_1)/(6k_3 - 6k_1)}$.

Moreover, when $N_z = 0$, numerical calculations reveal that g can have not any real zero, have one or two or three real zero(s), and different number of zeros results in different behavior. Consequently, the phase diagram for a helix can be divided into six regimes, as shown in Fig. 4.

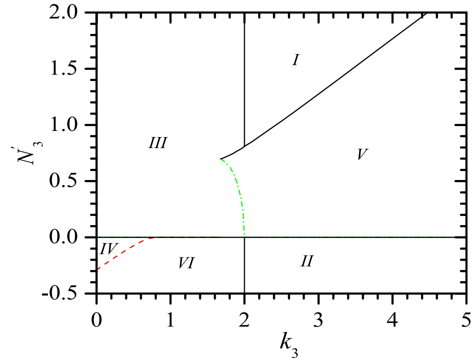

Fig. 4 Phase diagram for a helix when $k_1 = k_2 = 1$ and $N_z = 0$. The red dashed line is approximately $N_3' = -0.2831k_1 + 0.4022k_3$. The black solid oblique line is approximately $N_3' = -0.2286k_1 + 0.499k_3$. The vertical black line is given by $k_3 = 2$

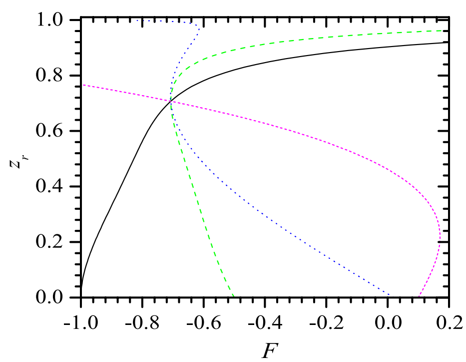

Fig. 5 z_r vs F for a helix when $k_3 = 2$ and $N_3' = 1$ (black solid); $k_3 = 2.5$ and $N_3' = -0.1$ (magenta short dashed); $k_3 = 1.5$ and $N_3' = 0.5$ (green dashed); $k_3 = 0.5$ and $N_3' = -0.02$ (blue dotted). $N_z = 0$ and $k_1 = k_2 = 1$ in all cases

In regime I, it has always $g > 0$ at any z_r so that a helix is always stable. The regime is bounded by $k_3 > 2$ and the black solid oblique line in Fig. 4. A typical sample is shown as the black solid line in Fig. 5.

In regime II, $g > 0$ when $z_{\mathrm{II}} > z_r$ so that a helix is stable when $z_{\mathrm{II}} > z_r > 0$ and it occurs when $k_3 > 2k_1$ and $N_3' < 0$. The larger the N_3', the smaller the z_{II}. The magenta short dashed line in Fig. 5 shows a typical sample in the regime. Note that z_{II} here is different from that in Sect. 3, and the same hints for other special values of z_r in the following texts.

In regime III, $g > 0$ when $z_r > z_{\mathrm{III}}$ so that a helix is stable when $z_r > z_{\mathrm{III}}$. This regime is bounded by $N_3' > 0$, $k_3 > 0$, the green dashed line, the black solid oblique line and the vertical black line in Fig. 4. The larger the N_3', the smaller the z_{III}. The green dashed line in Fig. 5 shows a typical sample in the regime.

In regime IV, $g \le 0$ when $z_r \le z_{\mathrm{IV}}^0$ or $z_r \ge z_{\mathrm{IV}}^1$ and $z_{\mathrm{IV}}^1 > z_{\mathrm{IV}}^0$. It follows that a helix is stable when $z_{\mathrm{IV}}^1 > z_r > z_{\mathrm{IV}}^0$ and the regime is bounded by $N_3' < 0$ and the red dashed line in Fig. 4. The larger the N_3', the smaller the z_{IV}^0 but the larger the z_{IV}^1. A typical sample is shown as the blue dotted line in Fig. 5.

In regimes I–IV, z_r increases monotonically with increasing F so that there is not sharp transition in z_r.

Regime V is special because in the regime z_r shows a shape transition at some F. In this regime, $g \le 0$ when $z_{\mathrm{V}}^2 \ge z_r \ge z_{\mathrm{V}}^1$ if $k_3 > 2k_1$ so g has two zeros, or $g \le 0$ when $z_{\mathrm{V}}^2 \ge z_r \ge z_{\mathrm{V}}^1$ or $z_r \le z_{\mathrm{V}}^0$ if $k_3 < 2k_1$ so g has three zeros. The larger the N_3', the larger the z_{V}^1 but the smaller the z_{V}^2. In other words, larger N_3' makes the transition sharper or more sensitive to force. The regime is bounded by $N_3' > 0$, the green dashed line and the black solid oblique line as shown in Fig. 4. Figure 6 shows a typical sample in the regime. Since g has two or three zeros, z_r is a triple-valued function of F when $z_{\mathrm{V}}^2 > z_r > z_{\mathrm{V}}^1$, as shown in Fig. 6. In the regime, $\mathcal{E} - F$ is self-crossed at $z_r = z_{\mathrm{E}}$, and the crossover point gives the lowest energy under a given F. Therefore, in a quasi-static process, z_r will jump suddenly at crossover point of $\mathcal{E}$. Moreover, tips in both $z_r - F$ and $\mathcal{E} - F$ curves define two metastable regimes, one is from z_{V}^1 to z_{E} and the other is from z_{E} to z_{V}^2. It means that in practice the discontinuous change in z_r will be more likely to occur at z_{V}^1 with increasing $|F|$, or occur at z_{V}^2 with decreasing $|F|$. The hysteresis indicates that the phase transition is first order. These behaviors are similar to those reported in Refs. (Zhou et al. 2005, 2007; Zhou 2018). Note that the transition occurs between two helices of different z_r, and it is different from a system with free BC (Zhou et al. 2017).

Finally, in regime VI, it has always $g < 0$ so that there is not helix. The regime is bounded by $N_3' < 0$, $k_3 < 2k_1$ and the red dashed line in Fig. 4.

On the other hand, when $N_3' = 0$,

$$g = k_3 - 2k_1 + 6(k_1 - k_3)z_r^2 + N_z/(1 - z_r^2)^{3/2}. \tag{44}$$

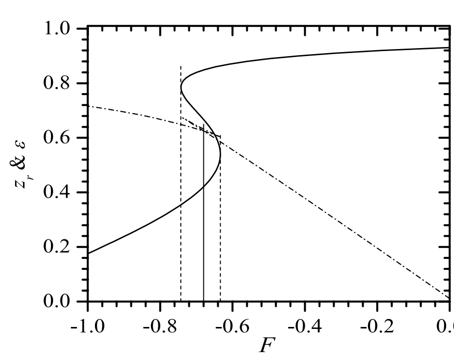

Fig. 6 z_r (solid) and $\mathcal{E}$ (dash dotted) vs F when $N_z = 0$, $k_1 = k_2 = 1$, $k_3 = 3.4$ and $N_3' = 1.28$. Two vertical dashed straight lines denote zeros of g and give z_{V}^1 and z_{V}^2. The vertical solid straight lines denote the crossover point of $\mathcal{E}$. $N_3 = 0$ in $\mathcal{E}$

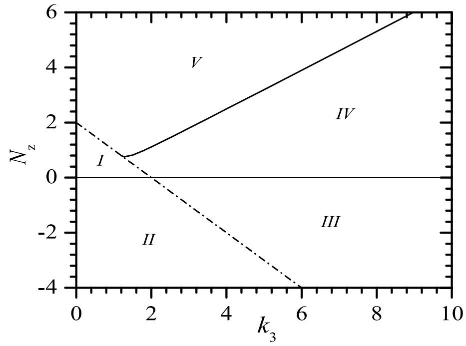

Fig. 7 Phase diagram for helix when $N_3' = 0$ and $k_1 = k_2 = 1$. The dash dotted line is given by $N_z + k_3 = 2k_1$. The solid line is approximately $N_z = -0.3098k_1 + 0.7045k_3$

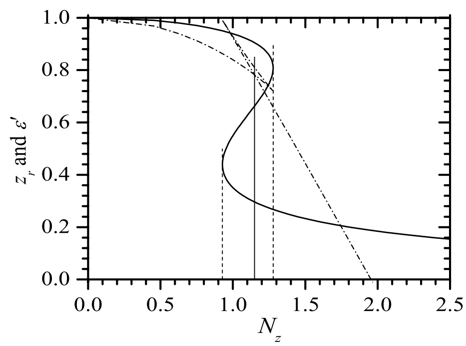

Fig. 8 z_r (solid) and $\mathcal{E}' = \mathcal{E} + 1.5$ (dash dotted) vs N_z when $N_3' = 0$, $k_1 = k_2 = 1$, $k_3 = 2.8$ and $F = 0.5$. $N_3 = 0$ in $\mathcal{E}$. Two vertical dashed straight lines denote where $G \equiv dN/dz_r = 0$, and the vertical solid straight lines denote the crossover point of $\mathcal{E}$

In this case, when $N_z = 0$, g has a real zero in $1 > z_r > 0$ when $2k_1 > k_3 > 8k_1/7$. When $z_r = 0$, $g = N_z + k_3 - 2k_1$ so that it requires $N_z + k_3 > 2k_1$ to have a helix with $z_r \sim 0$; when $z_r \sim 1$, $g \sim N_z/(1 - z_r^2)^{3/2}$ so that it requires $N_z > 0$ to form a helix with $z_r \sim 1$.

The phase diagram when $N_3' = 0$ is shown in Fig. 7. The phase diagram can be divided into five regimes separated by $N_z + k_3 = 2k_1$, $N_z = 0$ and the solid line in Fig. 7.

In regime I, $N_z + k_3 < 2k_1$ and $N_z > 0$, so that a helix is unstable when $z_r \sim 0$. In regime II, $N_z + k_3 < 2k_1$ and $N_z < 0$, so that a helix is unstable in either $z_r \sim 0$ or $z_r \sim 1$. In regime III, $N_z + k_3 > 2k_1$ and $N_z < 0$, so that a helix is unstable if $z_r \sim 1$. In regimes $I - -III$, F is a smooth function of z_r or there is not sharp transition in z_r.

Regime IV is bounded by $N_z + k_3 = 2k_1$, $N_z = 0$ and the solid line in Fig. 7. This regime is also special because g has two real zeros. Consequently, a helix with either a small z_r or large z_r is stable, but there exists a critical regime for z_r in which z_r has a first-order transition with varying F, similar to that shown in Fig. 6. Note that the range of this regime is similar to the regime V when $N_z = 0$, and it indicates that the sharp transition can still occur when both $N_z \neq 0$ and $N_3' \neq 0$.

Finally, the regime V is bounded by $N_z + k_3 = 2k_1$ and the solid line. In this regime, a helix is always stable and F is also a smooth function of z_r.

Moreover, when $N_3' = 0$, we find that with proper parameters and under a given F, N_z can induce a sharp change in z_r for a helix. A typical example is shown in Fig. 8. From Fig. 8, we can see that beginning from a moderate z_r, z_r is a triple-valued function of N_z and the $\mathcal{E} - N_z$ curve is self-crossed and the crossover point gives the lowest energy under a given N_z. It means that in the triple-valued regime, z_r will subject to a first-order transition, similar to that reported in Refs. (Zhou et al. 2007; Zhou 2018). Again, the transition occurs between two helices of different z_r but there is not such a transition for the system with a free $\psi(L)$ (Zhou et al. 2017).

In summary, when $k_1 = k_2$ and with a free $\psi(L)$, k_3 and N_3 are irrelevant to a helix. In contrast, when $\psi(L)$ is fixed, k_3 and N_3 are significant and result in rich phenomena owing to the coupling between bending and twisting. Particularly, a helix is in general a non-Hooke's spring, and its extension can subject to a first-order transition. N_3 and N_z play similar roles for the transition, and a large k_3 and positive torques favor such a transition.

When $k_1 \neq k_2$

In this case, in the same reason as that in subsection 3.2, taking a s-independent θ, the static equations become

$$\begin{aligned}&[k_3(1 - 2z_r^2) + (k_1 - k_2)(1 - z_r^2)\cos(2\psi)]\dot{\psi} \\ &\quad - 2(k_1 \sin^2\psi + k_2\cos^2\psi)z_r(1 - z_r^2)^{3/2} \\ &\quad + k_3 z_r(1 - 2z_r^2)\sqrt{1 - z_r^2} - N_3(1 - 2z_r^2) + N_z z_r \\ &\quad - F\sqrt{1 - z_r^2} = 0,\end{aligned} \tag{45}$$

$$2k_3\ddot{\psi} - (k_1 - k_2)(1 - z_r^2)^2 \sin(2\psi) = 0. \tag{46}$$

with BCs

$$\sin(2\psi) = 0,\ (k_3\dot{\psi} - N_3 + k_3 z_r\sqrt{1 - z_r^2})\delta\psi = 0. \tag{47}$$

Equation (45) is a first-order nonlinear differential equation in ψ, and Eq. (46) is a second-order nonlinear differential equation of ψ. It is straightforward to show that in general these two equations are incompatible when $k_1 \neq k_2$ and $\dot{\psi} \neq 0$. Therefore, to form a helix, from Eq. (46) we know that it has $\psi = 0$ or $\psi = \pi/2$.

Moreover, from Eq. (45), if $\psi = 0$ and $\psi(L)$ is free, we obtain

$$N_3 = k_3 z_r \sqrt{1 - z_r^2}, \tag{48}$$

$$F = -2k_2 z_r (1 - z_r^2) + N_z z_r / \sqrt{1 - z_r^2}. \tag{49}$$

Eqs. (48)–(49) are the same as those when $k_1 = k_2$, $\psi = 0$ and $C_\psi = 0$, i.e., Eqs. (38) and (40) with $\ddot{\theta} = 0$, $\psi = 0$ and $C_\psi = 0$. In other words, the behavior of the helix is the same as that with $N_3 = 0$, or anisotropy does not provide any new result.

Conclusions and discussions

In summary, we study the effects of two typical applied torques on the mechanical property of the helical configuration for an intrinsically straight filament in either three-dimensional space or on a cylinder. We obtain some algebraic static equations for a helix and find that the BCs affect the results seriously.

In 3D case, we find that for an isotropic filament, to have a stable helix requires that the twisting rigidity is larger than the bending rigidity. With free BCs or with a fixed $\phi(L)$, the filament becomes a Hooke's spring and a finite N_z is necessary but N_3 is irrelevant or the twisting is decoupled from bending. Since at a finite temperature and for a long filament, the thermal fluctuation will reduce the effects of BCs, we can conclude that N_3 is helpless in this case. On the other hand, fixing $\psi(L)$ results in a non-Hooke's spring which may exist only in a certain range of z_r and demands a complicate relation between γ and k_3. Moreover, with free BCs, anisotropy prohibits a helix, but with a fixed BC, the anisotropic filament becomes a non-Hooke's spring. In all cases, force is a monotonic function of extension so that there is not any abrupt change in extension for a 3D helix.

On the other hand, for an isotropic filament confined on a cylinder and when $\psi(L)$ is free, again N_3 is irrelevant in forming a helix. Consequently, at a finite temperature, k_3 and N_3 can also be ignored for a long filament. However, fixing $\psi(L)$ makes k_3 and N_3 crucial and results in rich behaviors. Particularly, in general the filament becomes a non-Hooke's spring, and with a large twisting rigidity and a large torque the extension of a helix can subject to a first-order transition. It is reasonable to expect that the similar phenomena will also occur in some other constrained systems. The transition occurs between two helices of different z_r so it may be relatively easier to be identified. For a biopolymer, fixing $\psi(L)$ can be realized by binding the end with some molecules, so that this finding is significant for a short rigid biopolymer since such a biopolymer can act as a switch or sensor in some biological processes.

Our findings support the conclusion that 'closed cylindrical confinement and chain stiffness are key factors for helical organization' of a biopolymers (Jung and Ha 2019). Our results also offer some insights into the conditions to form a helix for some semiflexible biopolymers. For instance, the conclusion that in free space to form a helix requires $k_3 > k_1$ suggests that a double-stranded DNA (dsDNA) may form a helix but a MreB molecule cannot, since $k_1/k_B T \approx 52 \pm 2$ nm and $k_3/k_B T \approx 75 \pm 25$ nm for a dsDNA, but $k_1/k_B T \approx 3.79 \times 10^6$ nm and $k_3/k_B T \approx 2.54 \times 10^6$ nm for a MreB molecule, where k_B is the Boltzmann constant and T is the temperature. However, inside a cylinder a MreB molecule can form a helix since its large k_3 favors a helix. Our findings may also be instructive to engineering since to fix Euler angles is analogous to prestress a filament and to build houses or bridges, it is commonly to use prestressed steel wires.

In this work, we do not consider the thermal and excluded volume effects. However, for an isotropic filament confined on a cylinder and with a free $\psi(L)$, it has been found that the thermal effect and excluded volume interaction play little role for a helix of moderate length (Zhou et al. 2017) and we expect that the same conclusion holds for the filament with a fixed $\psi(L)$. Moreover, for a filament confined on a cylinder, we do not consider the confinement from both ends of the cylinder in this work. It has been reported that such a confinement is crucial for a helix under a finite N_z (Zhou et al. 2017), so that the effect of the confinement is intrigue when N_3 is finite and it deserves a further investigation.

Acknowledgements This work has been supported by the MOST of China. Funding was provided by National Natural Science Foundation of China (Grant no. 11574256).

Appendix: Realization of two applied torques

In this appendix, we show how to realize external torques to obtain Eqs. (6) and (10). Meanwhile, we explain why $N_z s$ in Eqs. (6) and (10) are in fact different.

Relations between coordinates in different frames

First, note that in general the energy should be defined in a global fixed frame but the Euler angles are defined in local frames. We set the origin of the global fixed frame at $s = 0$, denote the relevant position vector to be $\mathbf{r}_g = (x_g, y_g, z_g)$ and the locus of the centerline to be $\mathbf{r}_c(s)$. The origin of the Euler frame, a local body frame, is at $\mathbf{r}_c(s)$. We denote further a position vector in Euler frame as $\mathbf{r}_E = (x_E, y_E, z_E)$ and define a local 'fixed' frame which has the same origin as that of the Euler frame but its three axes have the same orientations as those of the global fixed frame. In other words, 'fixed' means to fix the orientations of axes. Consequently, a position vector in the local 'fixed' frame is $\mathbf{r}_f = (x_f, y_f, z_f) = \lambda' \cdot \mathbf{r}_E$, where λ' is the transfer matrix of the rotation matrix λ with (Goldstein 2002)

$$\begin{aligned}
&\lambda_{11}(s) = \cos\phi\cos\psi - \cos\theta\sin\phi\sin\psi,\\
&\lambda_{12}(s) = \sin\phi\cos\psi + \cos\theta\cos\phi\sin\psi,\\
&\lambda_{13}(s) = \sin\psi\sin\theta,\\
&\lambda_{21}(s) = -\cos\phi\sin\psi - \cos\theta\sin\phi\cos\psi,\\
&\lambda_{22}(s) = -\sin\phi\sin\psi + \cos\theta\cos\phi\cos\psi,\\
&\lambda_{23}(s) = \cos\psi\sin\theta,\ \ \lambda_{31}(s) = \sin\theta\sin\phi,\\
&\lambda_{32}(s) = -\sin\theta\cos\phi,\ \ \lambda_{33}(s) = \cos\theta.
\end{aligned} \tag{50}$$

Clearly, for a general space point $\mathbf{r}_g = \mathbf{r}_c + \mathbf{r}_f$.

A torque along the axis of the filament

Applying a pair of forces $\mathbf{F}_E^{\pm} = (0, \pm F, 0)$ at $\mathbf{r}_E^{\pm} = (\pm l, 0, 0)$, respectively, these forces yield a torque$= N_3\mathbf{t}_3 = 2Fl\mathbf{t}_3$ in Euler frame. In global fixed frame, forces become $\mathbf{F}_g^{\pm} = \lambda'(L)\cdot\mathbf{F}_E^{\pm} = \pm F(\lambda_{21}(L), \lambda_{22}(L), \lambda_{23}(L))$ and they act at $\mathbf{r}_g(L)^{\pm} = \mathbf{r}_c(L) + \lambda'(L)\cdot(\pm l, 0, 0) = \mathbf{r}_c(L) \pm l(\lambda_{11}(L), \lambda_{12}(L), \lambda_{13}(L))$. When the filament undergoes a small deformation, the work done by these two forces is

$$\begin{aligned}
\mathrm{d}W &= \mathbf{F}_g^{+}\mathrm{d}\mathbf{r}_g^{+}(L) + \mathbf{F}_g^{-}\mathrm{d}\mathbf{r}_g^{-}(L)\\
&= N_3(\lambda_{21}\mathrm{d}\lambda_{11} + \lambda_{22}\mathrm{d}\lambda_{12} + \lambda_{23}\mathrm{d}\lambda_{13})\\
&= N_3[\cos\theta(L)\mathrm{d}\phi(L) + \mathrm{d}\psi(L)].
\end{aligned} \tag{51}$$

For a finite deformation via a path P, the corresponding energy is therefore

$$E_t = -N_3\int_P [\cos\theta(L)\mathrm{d}\phi(L) + \mathrm{d}\psi(L)]. \tag{52}$$

Since the energy is path-independent, we can choose the centerline of the filament as integral path, which leads to

$$E_t = -N_3\int_0^L \omega_3 \mathrm{d}s. \tag{53}$$

$\mathcal{E}_t = -N_3\omega_3$ is just the last term in Eqs. (6) and (10). It should be not too difficult to realize such a torque. If we fix $\phi(L)$, it becomes $\mathcal{E}_t = -N_3\dot{\psi}$. Moreover, from rotational symmetry, any torque along $\mathbf{t}_3$ yields the same energy term.

A torque along the fixed *z*-axis in 3D space

Now applying a pair of forces $\mathbf{F}_g^{\pm} = \pm F(-\sin\alpha, \cos\alpha, 0)$ at $\mathbf{r}_g(L)^{\pm} = \mathbf{r}_c(L) \pm l(\cos\alpha, \sin\alpha, 0)$, respectively, α is an angle around z-axis. It follows that the energy $\mathrm{d}E_t = -[\mathbf{F}_g^{+}\mathrm{d}\mathbf{r}_g(L)^{+} + \mathbf{F}_g^{-}\mathrm{d}\mathbf{r}_g(L)^{-}] = N_z\mathrm{d}\alpha = 2Fl\mathrm{d}\alpha$. Clearly, $\mathrm{d}\alpha = \mathrm{d}\phi(L) + \cos\theta(L)\mathrm{d}\psi(L)$ since $\phi(L)$ is also around z-axis but $\psi(L)$ is around $\mathbf{t}_3$ and $\cos\theta$ is the z-component of $\mathbf{t}_3$. Therefore, $\mathrm{d}E_t$ gives the third term in Eq. (6). It is also not too difficult to realize such a torque. With a fixed $\psi(L)$, it becomes $\mathcal{E}_t = -N_z\dot{\phi}$. From rotational symmetry, any torque along z-axis also yields the same term. However, it is very difficult to obtain such a torque from a single force because in this case the energy from $\mathbf{r}_c(L)$ becomes very complicate.

A torque along the cylinder axis

The third term in Eq. (10) has been used (Allard and Rutenberg 2009; Zhou et al. 2017) but it lacks a proper explanation on how to realize such a torque and it may be confused with the third term in Eq. (6) so that we clarify this point here.

On a cylinder, we can write $\mathbf{r}_g = \mathbf{r}_\perp + z\mathbf{e}_z$, where $\mathbf{r}_\perp = R(1-\cos\varphi)\mathbf{e}_x - R\sin\varphi\mathbf{e}_y$ and φ is yet unknown. Now we are applying a force $\mathbf{F}$ at $\mathbf{r}_g(L)$ and let $\mathbf{F}$ parallel to $\mathbf{t}_\perp = \sin\phi\ \mathbf{e}_x - \cos\phi\mathbf{e}_y$ or $\mathbf{F} = F(\sin\phi\ \mathbf{e}_x - \cos\phi\mathbf{e}_y)$. It follows that $d\mathbf{r}_\perp = R(\sin\varphi\mathbf{e}_x - \cos\varphi\mathbf{e}_y)\mathrm{d}\varphi$ is also parallel to $\mathbf{t}_\perp$ so that $\varphi = \phi$. The work done by this force is $\mathrm{d}W = \mathbf{F}\cdot\mathrm{d}\mathbf{r}_g(L) = \mathbf{F}\cdot\mathrm{d}\mathbf{r}_\perp(L) = FR\mathrm{d}\phi$. Therefore, the related energy density is $\mathcal{E}_t = -N_z\dot{\phi}(L)$ with $N_z = FR$ and it recovers the third term in Eq. (10).

Finally, note that this torque results from a single force so that it should be easier to realize than the N_z in Eq. (6) since it requires a pair of forces.

References

Allard JF, Rutenberg AD (2009) Pulling helices inside bacteria: imperfect helices and rings. Phys Rev Lett 102:158105

Andrews SS, Arkin AP (2007) A mechanical explanation for cytoskeletal rings and helices in bacteria. Biophys J 93:1872–1884

Benham CJ (1977) Elastic model of supercoiling. Proc Natl Acad Sci USA 74:2397–2401

Benham CJ (1989) Onset of writhing in circular elastic polymers. Phys Rev A 39:2582

Bustamante C, Marko JF, Siggia ED, Smith S (1994) Entropic elasticity of lambda-phage DNA. Science 265:1599–1600

Carballido-López R (2006) The bacterial actin-like cytoskeleton. Microbiol Mol Biol Rev 70:888–909

Chouaieb N, Goriely A, Maddocks JH (2006) Helices. Proc Natl Acad Sci USA 103:9398–9403

Daniel RA, Errington J (2003) Control of cell morphogenesis in bacteria: two distinct ways to make a rod-shaped cell. Cell 113:767–776

Erickson HP, Taylor DW, Taylor KA, Bramhill D (1996) Bacterial cell division protein FtsZ assembles into protofilament sheets and minirings, structural homologs of tubulin polymers. Proc Natl Acad Sci USA 93:519

Esue O, Wirtz D, Tseng Y (2006) GTPase activity, structure, and mechanical properties of filaments assembled from bacterial cytoskeleton protein MreB. J Bacteriol 188:968–976

Fain B, Rudnick J (1999) Conformations of closed DNA. Phys Rev E 60:7239

Fain B, Rudnick J, Östlund S (1997) Conformations of linear DNA. Phys Rev E 55:7364

Gitai Z, Dye N, Shapiro L (2004) An actin-like gene can determine cell polarity in bacteria. Proc Natl Acad Sci USA 101:8643–8648

Gitai Z, Dye N, Reisenauer A, Wachi M, Shapiro L (2005) MreB actin-mediated segregation of a specific region of a bacterial chromosome. Cell 120:329–341

Goldstein H (2002) Classical mechanics, 3rd edn. Addison-Wesley, Boston

Goriely A, Shipman P (2000) Dynamics of helical strips. Phys Rev E 6:4508

Iwai N, Nagai K, Wachi M (2002) Novel *S*-benzylisothiourea compound that induces spherical cells in *Escherichia coli* probably by acting on a rod-shape-determining protein(s) other than penicillin-binding protein 2. Biosci Biotechnol Biochem 66:2658–2662

Jones LJF, Carballido-López R, Errington J (2001) Control of cell shape in bacteria: helical, actin-like filaments in *Bacillus subtilis*. Cell 104:913–922

Jung Y, Ha BY (2019) Confinement induces helical organization of chromosome-like polymers. Sci Rep 9:869

Kessler DA, Rabin Y (2003) Stretching instability of helical springs. Phys Rev Lett 90:024301

Kratky O, Porod G (1949) Rontgenuntersuchung gelöster Fadenmoleküle. Recl Trav Chim Pays-Bas 68:1106

Kruse T, Bork-Jensen J, Gerdes K (2005) The morphogenetic MreBCD proteins of *Escherichia coli* form an essential membrane-bound complex. Mol Microbiol 55:78–89

Love AEH (1944) A treatise on the mathematical theory of elasticity. Dover, New York

Marko JF, Siggia ED (1994) Fluctuations and supercoiling of DNA. Science 265:506–508

Marko JF, Siggia ED (1998) Stretching DNA. Macromolecules 28:8759–8770

Moukhtar J, Fontaine E, Faivre-Moskalenko C, Arnéodo A (2007) Probing persistence in DNA curvature properties with atomic force microscopy. Phys Rev Lett 98:178101

Panyukov SV, Rabin Y (2000) Thermal fluctuations of elastic filaments with spontaneous curvature and torsion. Phys Rev Lett 85:2404

Panyukov SV, Rabin Y (2001) Fluctuating elastic rings: statics and dynamics. Phys Rev E 64:011909

Panyukov SV, Rabin Y (2002) On the deformation of fluctuating chiral ribbons. Europhys Lett 57:512–518

Russell JH, Keiler KC (2007) Peptide signals encode protein localization. J Bacteriol 189:7581–7585

Shih Y-L, Le T, Rothfield LI (2003) Division site selection in *Escherichia coli* involves dynamic redistribution of Min proteins within coiled structures that extend between the two cell poles. Proc Natl Acad Sci USA 100:7865–7870

Smith B, Zastavker YV, Benedek GB (2001) Tension-induced straightening transition of self-assembled helical ribbons. Phys Rev Lett 87:278101

Srinivasan R, Mishra M, Murata-Hori M, Balasubramanian MK (2007) Filament formation of the *Escherichia coli* actin-related protein, MreB, in fission yeast. Curr Biol 17:266–272

Srinivasan R, Mishra M, Wu L, Yin Z, Balasubramanian MK (2008) The bacterial cell division protein FtsZ assembles into cytoplasmic rings in fission yeast. Genes Dev 22:1741–1746

Starostin EL, van der Heijden GHM (2010) Tension-induced multistability in inextensible helical ribbons. Phys Rev Lett 101:084301

Taghbalout A, Rothfield L (2007) RNaseE and the other constituents of the RNA degradosome are components of the bacterial cytoskeleton. Proc Natl Acad Sci USA 104:1667–1672

Tanaka F, Takahashi H (1985) Elastic theory of supercoiled DNA. J Chem Phys 83:6017

Thanedar S, Margolin W (2004) FtsZ exhibits rapid movement and oscillation waves in helix-like patterns in *Escherichia coli*. Curr Biol 14:1167–1173

Vaillant C, Audit B, Arnéodo A (2005) Thermodynamics of DNA loops with long-range correlated structural disorder. Phys Rev Lett 95:068101

van der Heijden GHM (2001) The static deformation of a twisted elastic rod constrained to lie on a cylinder. Proc R Soc A 457:695–715

Vats P, Rothfield L (2007) Duplication and segregation of the actin (MreB) cytoskeleton during the prokaryotic cell cycle. Proc Natl Acad Sci USA 104:17795–17800

Zhou Z (2007) Elasticity of two-dimensional filaments with constant spontaneous curvature. Phys Rev E 76:061913

Zhou Z (2018) Novel relationships between some coordinate systems and their effects on mechanics of an intrinsically curved filament. J Phys Commun 2:035008

Zhou Z, Lai P-Y, Joós B (2005) Elasticity and stability of a helical filament. Phys Rev E 71:052801

Zhou Z, Joós B, Lai P-Y, Young Y-S, Jan J-H (2007) Elasticity and stability of a helical filament with spontaneous curvatures and isotropic bending rigidity. Mod. Phys. Lett. B 21:1895

Zhou Z, Lin F-T, Hung C-Y, Wu H-Y, Chen B-H (2014) Curvature induced discontinuous transition for semiflexible biopolymers. J Phys Soc Jpn 83:044802

Zhou Z, Joós B, Wu C-X (2017) Stability of the helical configuration of an intrinsically straight semiflexible biopolymer inside a cylindrical cell. AIP Adv 7:125003